Journal of Materials Chemistry

Dynamic Article Links

Cite this: *J. Mater. Chem.*, 2012, **22**, 20170

www.rsc.org/materials

COMMUNICATION

Discharge product morphology and increased charge performance of lithium–oxygen batteries with graphene nanosheet electrodes: the effect of sulphur doping†

Yongliang Li,[a] Jiajun Wang,[a] Xifei Li,[a] Dongsheng Geng,[a] Mohammad N. Banis,[a] Yongji Tang,[ab] Dongniu Wang,[ab] Ruying Li,[a] Tsun-Kong Sham[b] and Xueliang Sun*[a]

Received 18th July 2012, Accepted 15th August 2012
DOI: 10.1039/c2jm34718k

Sulphur-doped graphene was successfully fabricated and its influence on the discharge product formation in lithium–oxygen batteries was demonstrated. The growth and distribution of the discharge products were studied and a mechanism was proposed. This will have significant implication for cathode catalysts and rechargeable battery performance.

1. Introduction

Nonaqueous lithium–oxygen batteries have received much attention as a promising energy storage system beyond lithium-ion batteries (LIBs) for electric vehicles (EVs) due to their extremely high specific energy densities which could be 5–10 times higher than those of LIBs.[1] However, one critical challenge for the practical application of lithium–oxygen batteries is to develop an optimal porous cathode since the insoluble product, lithium peroxide (Li_2O_2), deposits in and eventually will clog the electrode pores which limits the discharge capacity.[2] Another challenge is the poor rate capability and significant polarization of cell voltage which is also due to the formation of Li_2O_2. Recent studies reported that the structure, composition, and electronic properties of the discharge product, Li_2O_2, of lithium–oxygen batteries could dramatically affect the battery performance. For example, Nanda *et al.* found that the distribution of lithium products in lithium–oxygen cathodes significantly affected the rechargeability of the batteries.[3] Luntz *et al.* suggested that sudden death occurred from the limited charge transport through the growth of Li_2O_2 films.[4] Seriani proposed that the particle size of lithium oxides had an impact on the porous electrodes.[5] Siegel *et al.* found that the surface electronic structure of small Li_2O_2 particles was dramatically different from that of the bulk insulator due to the lithium vacancies.[6] Ceder *et al.* further demonstrated that the electronic conduction was likely to be controlled by vacancy diffusion in Li_2O_2.[7]

Toward the goal of tailoring Li_2O_2 properties to battery performance, it is very important to select or design the optimal growth of Li_2O_2 *via* substrate control. In our previous report, we had found that nitrogen-doped graphene showed significant influence not only on the battery performance but also on the nucleation and growth of discharge products, which is that more small and uniform particles were obtained.[8] Therefore, it is interesting to investigate the properties of other heteroatom doped graphenes. Recently, Huang *et al.* reported sulphur-doped graphene as an electrocatalyst for oxygen reduction reaction (ORR) and found that the sample exhibited excellent catalytic activity, long-term stability, and high methanol tolerance.[9] However, to the best of our knowledge, sulphur-doped graphene has rarely been employed in the nonaqueous lithium–oxygen battery system. Herein, we successfully fabricated sulphur-doped graphene and demonstrate its influence on Li_2O_2 formation. The experimental results not only give further insight into the reaction mechanism but also provide a rational direction to modify cathode material properties for lithium–oxygen batteries. This will also have significant implication for catalysts performance at the cathode.

2. Experimental

2.1 Materials synthesis

Graphene nanosheets (GNSs) were prepared by the oxidation of graphite powder using the modified Hummers' method, and sulphur-doped graphene (S-GNSs) was subsequently obtained using the following procedure: 0.05 g of graphene was dispersed into acetone with 0.8 g of *p*-toluenesulfonic acid (Alfa Aesar). Then the slurry was stirred at room temperature until the solvent totally evaporated. The resulting product was dried at 100 °C overnight and finally calcined at 900 °C in Ar for 1 hour.[10]

2.2 Physical characterizations

The morphologies of GNSs, S-GNSs and the discharge products were characterized by a Hitachi S-4800 FESEM. XRD patterns were

[a]*Department of Mechanical and Materials Engineering, University of Western Ontario, London, Ontario, Canada, N6A 5B9. E-mail: xsun@eng.uwo.ca; Fax: +1-519-6613020; Tel: +1-519-6612111 ext. 87759*
[b]*Department of Chemistry, University of Western Ontario, London, Ontario, Canada, N6A 5B7*

† Electronic supplementary information (ESI) available: SEM image of graphene, Raman spectroscopy of sulphur-doped and pristine graphene. SEM image and XRD pattern of discharge products after the 2nd cycle. See DOI: 10.1039/c2jm34718k

recorded by a Bruker-AXS D8 Discover diffractometer (Co-Kα source). XPS spectra were obtained using a Kratos Axis Ultra X-ray photoelectron spectrometer (Al Kα source). Raman scattering (RS) spectra were recorded on a HORIBA Scientific LabRAM HR Raman spectrometer system equipped with a 532.4 nm laser. The S K-edge XANES spectra were obtained on the Soft X-ray Micro-characterization Beamline (SXRMB, $\Delta E/E$: 10^{-4}) while the Li K-edge spectra were obtained on the Variable Line-Spacing Planar Grating Monochromator beamline (VLS-PGM, $\Delta E/E$: 10^{-5}) at the Canadian Light Source (CLS). Reference samples, sulphur, Li_2O_2 and Li_2CO_3 were purchased from Sigma-Aldrich and used without further purification. Spectra were recorded in fluorescence yield mode (FLY).

2.3 Electrochemical measurements

Swagelok type cells were used to test the battery performance. GNSs or S-GNSs and polyvinylidene fluoride (PVDF) (Alfa Aesar, 98.5%) with a weight ratio of 9 : 1 were cast onto a separator (Celgard 3500) and cut to 3/8 inch in diameter as the cathode and the material loadings were ~0.3 mg. 1 mol dm^{-3} $LiPF_6$–tetraethylene glycol dimethyl ether (TEGDME) was used as the electrolyte. The discharge–charge characteristics were measured using an Arbin BT-2000 battery station in the voltage range of 2.0–4.5 V in a 1 atm oxygen atmosphere at 25 °C.

3. Results and discussion

Fig. 1a shows the SEM image of S-GNSs. It can be seen that it features a curly morphology with a thin, wrinkled structure which is similar to pristine graphene (ESI, Fig. S1†). The elemental composition was analyzed by EDX mapping (Fig. 1b). The presence of sulphur is confirmed and the sulphur distribution in the graphene is relatively uniform, suggesting that sulphur atoms are not only in plane but also at the edge of GNSs. XPS further confirms that sulphur is successfully doped into graphene, and the sulphur percentage is about 1.9 at% (Fig. 1c). The high-resolution S 2p peak is shown in the inset of Fig. 1c. As can be seen, covalent C–S bonds were doped in two forms. One is –C–S–C– (163.8 eV) and the other is –C–SO_x– (x = 2–4, 165.0–166.5 eV), such as sulfate or sulfonate.[9,11] The synchrotron-based XANES spectroscopy is a molecular-scale technique that yields local electronic and structural information on the element of interest.[12] The sulphur doping is supported by S K-edge XANES as shown in Fig. 1d; the intense peak at 2473.2 eV can be assigned to a transition of S 1s to a S–C final state of p character while the broad peak between 2480 and 2482 eV could be attributed to a mixture of sulphur of valences 4^+ (sulfone) and 5^+ (sulfonate).[13] Based on the XPS and XANES results, we can conclude that sulphur was doped into the framework of graphene, although the exact position of substitutional sulphur requires further study.

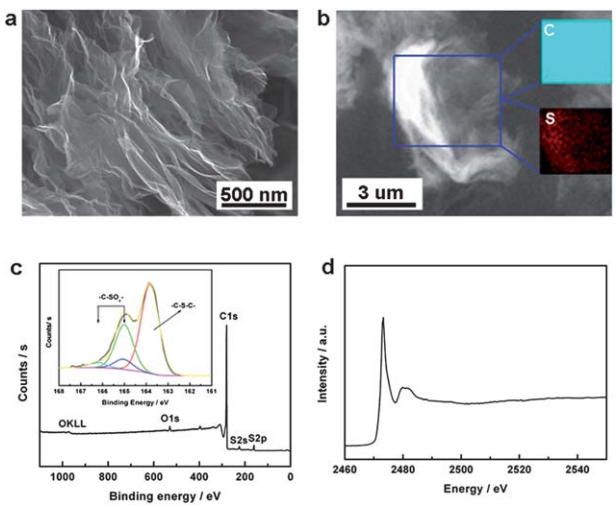

Fig. 1 (a) SEM image, (b) EDS mapping, (c) XPS spectroscopy, and (d) S K-edge XANES of sulphur-doped graphene.

The Raman spectra of sulphur-doped and pristine graphene are shown in the ESI, Fig. S2.† Both samples display two peaks at ~1353 and 1598 cm^{-1}, which correspond to the D band and G band, respectively. It is well accepted that higher disorder (more defects) leads to a higher intensity ratio between the D band and G band.[14] For S-GNSs, the I_D/I_G ratio increases to about 1.06 from a value of around 0.96 for pristine graphene. In addition, the spectra also exhibit a broadening of the D band for the S-GNSs, implying an enhanced defect density. In our previous effort on the fabrication of heteroatom-doped graphene for lithium–oxygen batteries, we found that the discharge capacity dramatically increased resulting from the introduction of defective sites (defects or functional groups) after nitrogen doping.[8] However, as can be seen from Fig. 2a and b, the initial discharge capacity of S-GNS electrode is about 4300 mA h g^{-1}, which is lower than that of the pristine graphene electrode (~8700 mA h g^{-1}). However, it is noted that the initial charge capacity of the S-GNS electrode is about 4100 mA h g^{-1}, while it is only around 170 mA h g^{-1} for the pristine graphene electrode. Moreover, the discharge capacities in the second cycle of the sulphur-doped and pristine graphene electrodes are 3500 and 220 mA h g^{-1}, respectively. It was reported by Shao-Horn's group that the catalytic activity of the catalysts towards oxygen reduction reaction, affecting the discharge performance of lithium–oxygen batteries, was related to the oxygen adsorption energy.[15] But the first-principle calculations showed that the oxygen adsorption energy was not increased by doping sulphur into graphene.[16] Therefore, the discharge capacity of S-GNSs for lithium–oxygen batteries could not be improved based on the merely increased adsorption ability for oxygen; the reason that it shows lower discharge capacity but higher charge capacity will be further discussed below.

Fig. 3a and b show the SEM morphologies of the discharge products for sulphur-doped and pristine graphene electrodes, respectively. It can be seen that the discharge products were deposited on the entire porous electrodes for both samples, but the morphologies are significantly different. Irregular-shaped particles formed on the pristine graphene electrode while, interestingly, nanorods with a

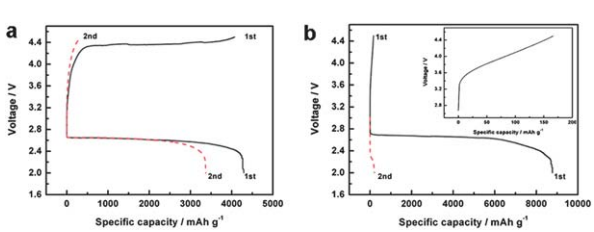

Fig. 2 Discharge–charge curves of (a) sulphur-doped and (b) pristine graphene electrodes at a current density of 75 mA g^{-1}. Inset of (b) is an enlarged figure of the charge curve for the 1st cycle.

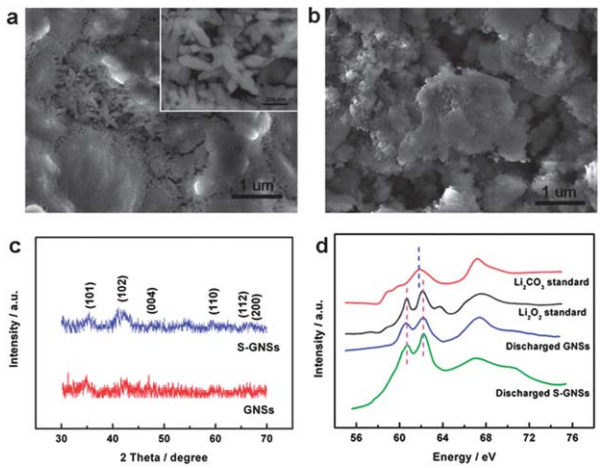

Fig. 3 SEM images of (a) sulphur-doped and (b) pristine graphene discharged electrodes. (c) XRD patterns and (d) XANES of discharge products of S-GNSs.

diameter of about 100 nm grew on the S-GNS electrode. The discharge products of the two electrodes were examined by XRD and the patterns are shown in Fig. 3c. It is interesting to find that the XRD peaks can be assigned to Li_2O_2, although the morphology of the discharge product on S-GNSs is different. In our previous report, we found that the discharge product on pristine and nitrogen-doped graphene was Li_2O_2, which is consistent with the results obtained by other groups.[8] The discharge product on S-GNSs is better crystallized than that on pristine graphene, suggesting that the dismutase reaction and nucleation of Li_2O_2 are promoted due to the strong interaction between carbon and the intermediate products after sulphur doping.[17] The Li K-edge XANES spectra of the discharge product for GNS, S-GNS electrodes and reference materials, such as standard Li_2CO_3 and Li_2O_2, are shown in Fig. 3d. As can be seen, two major peaks at ~60.8 and ~62.2 eV are present for both GNS and S-GNS samples, which match well with the standard Li_2O_2 material, while an additional peak at ~63.7 eV was observed for the reference. However, it is much different from that of Li_2CO_3 (only one peak at ~61.8 eV). It is reported that the Li^+ local environment in the Li_2O_2 of discharged pure carbon powder and Au/C electrodes is different from that of the standard bulk materials which is due to the presence of structural defects such as oxygen and/or lithium vacancies.[17] The broadening of the doublet is consistent with this notion (increasing disorder compared with the reference). The SEM image of the discharge products after the 2nd discharge is shown in the ESI, Fig. S3a.† As can be seen, nanorod-shaped structures still appear, however, the diameter of the nanorods is smaller compared to that of the products formed after the 1st discharge. It can be seen from the XRD pattern that in addition to Li_2O_2, Li_2CO_3 is also present, indicating the side reactions of the electrolyte during the discharge–charge cycle (ESI, Fig. S3b†).[18] The decreased charge capacity in the 2nd cycle is due to the Li_2CO_3 formation which increases the polarization in the electrode (higher charging voltage is needed to decompose Li_2CO_3).[19]

Several works have demonstrated that sulphur can be used as the catalyst for nanostructural formation or determine the morphology of nanomaterials, such as cementite,[20] ZnO,[21] SnO_2,[22] however, there is no literature on the nanostructural formation of lithium oxides. It is reported that S-doped graphene can act as a semiconductor compared to the pristine one, resulting in an increased electrode polarization in the battery.[23] This will diminish the binding of the generated O_2^- to the substrate during discharge, thus enhancing the diffusion of the superoxide molecules away from the electrode surface, and favouring the disproportional peroxide formation, leading to a nanorod-shape structure growth.[18] However, the exact role of sulphur in the growth of the nanorod will need further study. The discharge current density is the same for the sulphur-doped and pristine graphene; the particle-shaped discharge product would have a higher packing density on the deposition surface compared to nanowires/nanorods.[24] Therefore, the amount of the discharge product on the S-GNSs is less than that on the pristine one, indicating a lower discharge capacity as well. However, the dense layer of Li_2O_2 on pristine graphene significantly affects the charge transport through the Li_2O_2–electrolyte interface, and thus the charge performance. In contrast, for S-GNSs, the randomly distributed Li_2O_2 nanorods will provide sufficient tunnelling holes that support the electrochemical reaction during the charge process, leading to an increased charge performance.[4]

The growth of the Li_2O_2 nanorods was observed by controlling the discharge depth of the batteries while keeping the discharge current density at 75 mA g^{-1}. Fig. 4a–c show the SEM images of the discharged electrodes. It can be seen that at 2.6 V, nanorods had already grown on most of the surface of the electrode and the diameter is around 35 nm. As the discharge voltage decreased, the electrode surface was all covered with the nanorods and the diameters

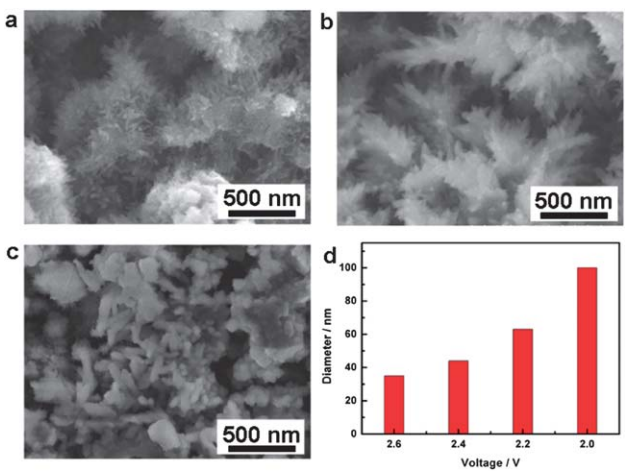

Fig. 4 SEM images of discharged S-GNS electrodes at (a) 2.6 V, (b) 2.4 V and (c) 2.2 V at a current density of 75 mA g^{-1}; (d) mean diameters of the discharge products.

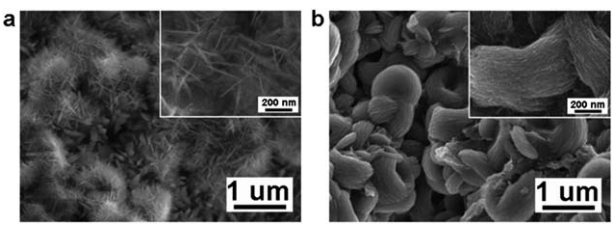

Fig. 5 SEM images of discharge products at current densities of (a) 150 mA g^{-1}, (b) 300 mA g^{-1}. Insets of (a) and (b) are the high-magnification images.

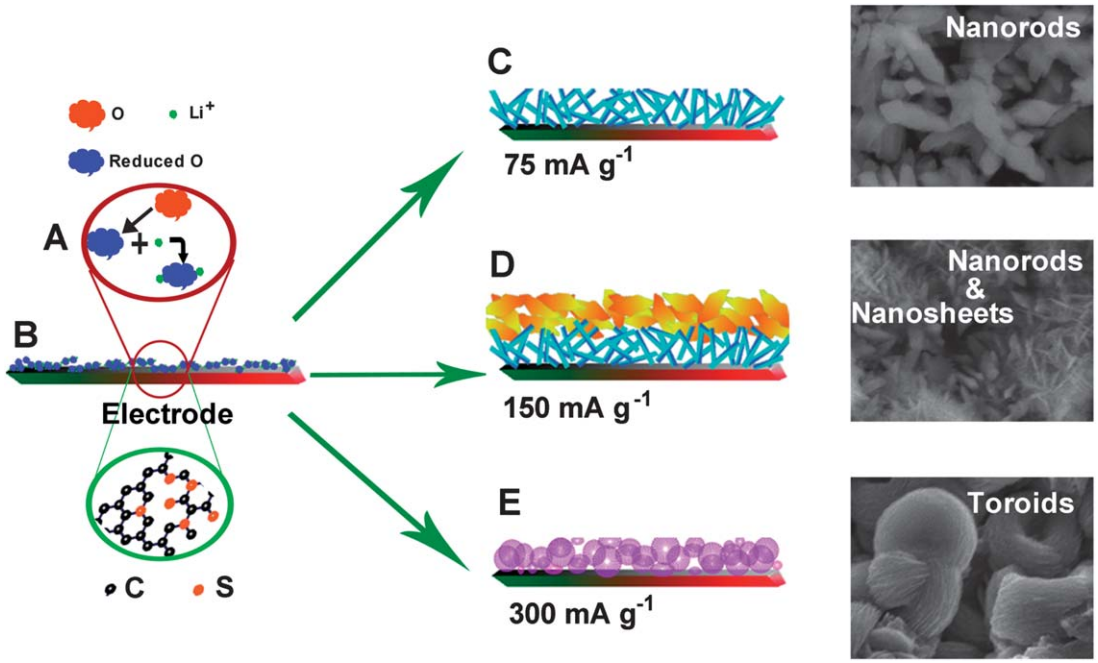

Fig. 6 Schematic of the growth of discharge product nanostructures on S-GNS electrodes.

increased to ~45,~75 and ~100 nm at 2.4, 2.2 and 2 V, respectively (Fig. 4d). However, the morphology of the discharge product changed when higher current densities were applied. As shown in Fig. 5a, in addition to the nanorods on the electrode surface, nanosheets with a thickness of ~10 nm were formed on the nanorods at 150 mA g^{-1}. Donut-shaped particles on the order of ~1 μm were found instead of nanorods or nanosheets at 300 mA g^{-1} (Fig. 5b). These toroidal particles were composed of aggregated nanosheet-structures; these toroids were also found by other groups but the formation and structural evolution have not been observed before.[18]

From our study by employing S-GNS electrode, the growth mechanism of the discharge product can be proposed based on the experimental results. Fig. 6 shows the schematic of the growth mechanism. Initially, O_2 is reduced to O_2^- and combined with Li^+ to form LiO_2 (Fig. 6A). Then elongated nanocrystallites of Li_2O_2 form on the carbon surface (Fig. 6B). Depending on the discharge current density, different morphologies are obtained. At a current density of 75 mA g^{-1}, only Li_2O_2 nanorods were formed (Fig. 6C). As the current density increases to 150 mA g^{-1}, the cathodic polarization increases which enhances the diffusion of the superoxide molecules away from the electrode surface, and peroxide forms along certain facets of the Li_2O_2 crystal, thus nanosheets were observed on nanorods (Fig. 6D). If a current density of 300 mA g^{-1} was applied, the cathodic polarization increased even more, and instead of the formation of nanorods, only nanosheets formed and gave rise to the toroid aggregates of Li_2O_2 (Fig. 6E). Nazar *et al.* suggested that Li_2O_2 favoured growth on the sites where the superoxide is generated in order to shorten the O_2^- diffusion path which may support our hypothesis.[18] However, in the real system, the growth is surely more complicated and further studies are needed to verify the hypothesis.

4. Conclusions

In summary, we have employed S-GNSs as cathode materials for lithium–oxygen batteries and found that the morphology of the discharge product, Li_2O_2, and therefore the discharge and charge properties of the batteries were significantly different from those of pristine graphene. The formation of Li_2O_2 nanorods during discharge and thus the charge properties are considered to be due to sulphur-doping; however, the role that sulphur played is not clear at the current stage and further study is needed. The detailed morphological evolution of Li_2O_2 as a function of the discharge depth and current density is also demonstrated for the first time. This study gives a rational direction for selecting and designing cathode materials (including catalysts) to tailor the morphology of Li_2O_2, thus improving the performance of lithium–oxygen batteries.

Notes and references

1 K. Abraham and Z. Jiang, *J. Electrochem. Soc.*, 1996, **143**, 1; M. Armand and J.-M. Tarascon, *Nature*, 2008, **451**, 652.
2 J. Xiao, D. Wang, W. Xu, D. Wang, R. Williford, J. Liu and J.-G. Zhang, *J. Electrochem. Soc.*, 2010, **157**, A487; Y. Li, J. Wang, X. Li, J. Liu, D. Geng, J. Yang, R. Li and X. Sun, *Electrochem. Commun.*, 2011, **13**, 668; S. Zhang, D. Foster and J. Read, *J. Power Sources*, 2010, **195**, 1235; Y. Li, J. Wang, X. Li, D. Geng, R. Li and X. Sun, *Chem. Commun.*, 2011, **47**, 9438.
3 J. Nanda, H. Bilheux, S. Voisin, G. M. Veith, R. Archibald, L. Walker, S. Allu, N. Dudney and S. Pannala, *J. Phys. Chem. C*, 2012, **116**, 8401.
4 V. Viswanathan, K. S. Thygesen, J. S. Hummelshøj, J. K. Nørskov, G. Girishkumar, B. D. McCloskey and A. C. Luntz, *J. Chem. Phys.*, 2011, **135**, 214704.
5 N. Seriani, *Nanotechnology*, 2009, **20**, 445703.
6 M. D. Radin, J. F. Rodriguez, F. Tian and D. J. Siegel, *J. Am. Chem. Soc.*, 2012, **134**, 1093.
7 S. P. Ong, Y. Mo and G. Ceder, *Phys. Rev. B: Condens. Matter Mater. Phys.*, 2012, **85**, 081105.
8 Y. Li, J. Wang, X. Li, D. Geng, M. N. Banis, R. Li and X. Sun, *Electrochem. Commun.*, 2012, **18**, 12.
9 Z. Yang, Z. Yao, G. Li, G. Fang, H. Nie, Z. Liu, X. Zhou, X. Chen and S. Huang, *ACS Nano*, 2012, **6**, 205.
10 D. Geng, Y. Chen, Y. Chen, Y. Li, R. Li, X. Sun, S. Ye and S. Knights, *Energy Environ. Sci.*, 2011, **4**, 760; D. Geng, S. Yang,

Y. Zhang, J. Yang, J. Liu, R. Li, T.-K. Sham, X. Sun, S. Ye and S. Knights, *Appl. Surf. Sci.*, 2011, **257**, 9193; H. C. Schniepp, J.-L. Li, M. J. McAllister, H. Sai, M. Herrera-Alonso, D. H. Adamson, R. K. Prud'homme, R. Car, D. A. saville and I. A. Aksay, *J. Phys. Chem. B*, 2006, **110**, 8535; X. Li, D. Geng, Y. Zhang, X. Meng, R. Li and X. Sun, *Electrochem. Commun.*, 2011, **13**, 822.

11 P. A. Denis, R. Faccio and A. W. Mombru, *ChemPhysChem*, 2009, **10**, 715; S. Glenis, A. J. Nelson and M. M. Labes, *J. Appl. Phys.*, 1999, **86**, 4464.

12 S. Yang, D. Wang, G. Liang, Y. Yiu, J. Wang, L. Liu, X. Sun and T.-K. Sham, *Energy Environ. Sci.*, 2012, **5**, 7007; D. Wang, J. Yang, X. Li, J. Wang, R. Li, M. Cai, T. K. Sham and X. Sun, *Cryst. Growth Des.*, 2012, **12**, 397.

13 G. N. George and M. L. Gorbaty, *J. Am. Chem. Soc.*, 1989, **111**, 3182; T. A. Smith, J. G. DeWitt, B. Hedman and K. O. Hodgson, *J. Am. Chem. Soc.*, 1994, **116**, 3836; P. Frank, S. D. George, E. Anxolabéhère-Mallart, B. Hedman and K. O. Hodgson, *Inorg. Chem.*, 2006, **45**, 9864.

14 Y. Shao, S. Zhang, M. H. Engelhard, G. Li, G. Shao, Y. Wang, J. Liu, I. A. Aksay and Y. Lin, *J. Mater. Chem.*, 2010, **20**, 7491; D. Deng, X. Pan, L. Yu, Y. Cui, Y. Jiang, J. Qi, W. Li, Q. Fu, X. Ma, Q. Xue, G. Sun and X. Bao, *Chem. Mater.*, 2011, **23**, 1188; Z. Wu, W. Ren, L. Gao, J. Zhao, Z. Chen, B. Liu, D. Tang, B. Yu, C. Jiang and H. Chen, *ACS Nano*, 2009, **3**, 411; H. Wang, C. Zhang, Z. Liu, L. Wang, P. Han, H. Xu, K. Zhang, S. Dong, J. Yao and G. Cui, *J. Mater. Chem.*, 2011, **21**, 5430.

15 Y.-C. Lu, H. A. Gasteiger and Y. Shao-Horn, *J. Am. Chem. Soc.*, 2011, **133**, 19048.

16 J. Dai, J. Yuan and P. Giannozzi, *Appl. Phys. Lett.*, 2009, **95**, 232105.

17 Y.-C. Lu, D. G. Kwabi, K. P. C. Yao, J. R. Harding, J. Zhou, L. Zuin and Y. Shao-Horn, *Energy Environ. Sci.*, 2011, **4**, 2999.

18 S. Freunberger, Y. Chen, N. Drewett, L. Hardwick, F. Bardé and P. Bruce, *Angew. Chem., Int. Ed.*, 2011, **50**, 1; R. Black, S. H. Oh, J.-H. Lee, T. Yim, B. Adam and L. F. Nazar, *J. Am. Chem. Soc.*, 2012, **134**, 2902; R. R. Mitchell, B. M. Gallant, C. V. Thompson and Y. Shao-Horn, *Energy Environ. Sci.*, 2011, **4**, 2952.

19 A. Thapa, K. Saimen and T. Ishihara, *Electrochem. Solid-State Lett.*, 2010, **13**, A165.

20 J. Hucińska, *Mater. Corros.*, 2004, **55**, 292.

21 G. Ambrožič, I. Djerdj, S. D. Škapin, M. Žigon and Z. C. Orel, *CrystEngComm*, 2010, **12**, 1862.

22 S. de Monredon, A. Cellot, F. Ribot, C. Sanchez, L. Armelao, L. Gueneau and L. Delattre, *J. Mater. Chem.*, 2002, **12**, 2396.

23 P. Kulkarni, L. Porter, F. Koeck, Y.-J. Tang and R. Nemanich, *J. Appl. Phys.*, 2008, **103**, 084905; P. Denis, R. Faccio and A. Mombru, *ChemPhysChem*, 2009, **10**, 715.

24 G. Cao and Y. Wang, *Nanostructures and Nanomaterials: Synthesis, Properties and Applications*, World Scientific Publishing, Hackensack, New York, 2011.

